3D solution structure of copper and silver-substituted yeast metallothioneins+

Cynthia W. Peterson[a], Surinder S. Narula[b,c], Ian M. Armitage[b,*]

[a]Physics Department, Univ. of Connecticut, Storrs, CT 06269-3046, USA
[b]Department of Pharmacology, Yale University School of Medicine, 333 Cedar Street, P.O. Box 208066, New Haven, CT 06520-8066, USA
[c]Ariad Pharmaceuticals, Cambridge, MA 02139, USA

Received 3 August 1995; revised version received 4 December 1995

Abstract 3D solution structural calculations for yeast silver(I)-substituted metallothionein (MT) and native copper(I) MT were completed using experimentally determined NOE and dihedral angle constraints, in conjunction with experimentally derived metal-to-Cys connectivities for AgMT which were assumed identical for CuMT. For the first 40 residues in both structures, the polypeptide backbone wraps around the metal cluster in two large parallel loops separated by a deep cleft containing the metal cluster. Minor differences between the two structures include differences in hydrogen bonds and the orientation of the N-terminus with the overall protein volume conserved to within 6.5%.

Key words: Yeast metallothionein; Protein structure; Nuclear magnetic resonance

1. Introduction

Metallothioneins (MTs) are ubiquitous metal-rich proteins characterized in all homologies by an abundance of cysteine residues and lack of generic structural motifs, α-helix and β-sheet [1]. The yeast protein, though differing in the number of cysteine residues and metal content from the structurally well-characterized mammalian MT proteins, nevertheless, serves a similar function in primary metal storage, transport and detoxification [2]. Additional evidence associates MT in host defense processes, radiative resistance and abnormal metal metabolism in inherited disease states such as leukemia and Menke's disease [3].

The native yeast *Saccharomyces cerevisiae* MT binds Cu(I), for which recent data supports a single polynuclear metal cluster [4]. Recent 2D ^{1}H and ^{1}H-^{109}Ag heteronuclear multiple-quantum coherence (HMQC) NMR experiments on the isomorphic, magnetically active (I = 1/2) Ag(I)-substituted yeast MT provided the requisite metal-to-Cys connectivities required for this protein's solution structure elucidation [5,6]. Additional structural constraints from NOE and coupling constant data for both the Ag(I) and the native Cu(I) protein were subsequently reported [7]. Assuming conserved metal-to-Cys connectivities, these data have now been used to calculate the full 3D solution structure of the native Cu(I) and Ag(I)-substituted yeast MT.

As was the case for the mammalian MTs, the structure determination of yeast MT was hampered by the paucity of NOE constraints due to the fact that the secondary structure of MT is dictated entirely by metal ligation, with the absence of regular secondary structural features. An additional factor, is the limited number (11 in yeast) of different amino acid residues and the lack of aromatic residues although in this regard, yeast MT is unique in that it contains a single histidine residue. The potential involvement of this histidine residue in metal binding, however, has been excluded by the HMQC studies [7]. For all of these reasons, yeast MT has a relatively low number of NOEs/residue which places an even greater weight on the significant role of the few medium and long range NOEs in establishing this protein's tertiary structure.

The calculated structure of both AgMT and CuMT involves the folding of the polypeptide backbone around a single cluster of seven metal atoms in two large, parallel protein loops, resembling a sprung paperclip whose parallel loops are no longer coplanar. A deep cleft between the loops contains the metal cluster with only the metals on the open side of the cleft exposed to solvent. Similarities and differences between the structure of AgMT and CuMT are delineated.

The yeast MT metal cluster has often been cited as a structural model for the metal cluster of the ACE1 regulatory protein [8]. Both share a common stoichiometry of metal ions bound in a cooperatively formed, Cu-thiolate cluster which provides resistance to proteinase digestion and exhibits a room temperature luminescence spectrum consistent with a metal cluster partially shielded from solvent quenching. It has been suggested that the larger ionic radius of Ag resulted in a less compact structure and greater solvent exposure of the Ag cluster in AgACE1 compared with CuACE1, to account for the shorter luminescent lifetime [9], less cooperative metal binding and reduced DNA affinity [10], and lower stability and smaller size of the protected peptide in proteolysis experiments [11]. The present study provides the first opportunity to compare the experimentally determined structures of the structurally homologous yeast Ag and CuMT.

*Corresponding author. *Present address:* Department of Biochemistry, University of Minnesota, Minneapolis, MN 55455, USA.
Fax: (1) (612) 625-2163. E-mail: ian@dimer.biochem.umn.edu

Abbreviations: AgMT, silver(I)-substituted yeast metallothionein; AgT48, silver(I)-substituted yeast mutant metallothionein; COSY, homonuclear two-dimensional correlation spectroscopy; CuMT, copper(I) yeast metallothionein; EXAFS, extended X-ray absorption fine structure; HMQC, heteronuclear multiple-quantum coherence spectroscopy; MT, metallothionein; NMR, nuclear magnetic resonance; NOE, nuclear Overhauser effect; rmsd, root mean square deviation.

SSDI 0014-5793(95)01492-6

2. Materials and methods

2.1. Distance and angle restraints

Distance and angle restraints were extracted from the reported experimental NMR data [6,7]. For AgMT, there are a total of 220 NOE constraints consisting of 60 intraresidue, 145 short range interresidue and 15 long range as summarized in Fig. 1a. For CuMT, there are a total of 203 NOE constraints: 61 intraresidue, 122 short range interresidue and 20 long range which are summarized in Fig. 1b.

The distance constraints from NOE mixing times of 80 ms for AgMT and 60 ms for CuMT were classified into strong, medium and weak NOEs, corresponding to 1.8–2.7 Å, 1.8–3.2 Å, 1.8–3.6 Å, respectively [12,13]. An additional 1.0 Å was added to the upper limit for NOEs involving methyl groups or non-stereospecifically assigned H^{β}s [5] and 0.5 Å was added for Ala amide proton to methyl proton NOEs [14,15]. In a separate experiment with a longer mixing time (150 ms), additional very weak NOEs were observed corresponding to 1.8–4.5 Å. Fig. 2 summarizes the sequential and medium range NOE connectivities and their strengths, slowly exchanging amide protons, half turns, Type I turns, $^3J_{HN\alpha}$ coupling constants used to provide the backbone dihedral angle constraints, experimentally determined metal-Cys coordinate bonds on AgMT by HMQC methods and all the long range NOEs observed for (a) AgMT and (b) CuMT. For $^3J_{HN\alpha}$ = 5, 6 to 8, 9 and 10 Hz, the ϕ values were $-60 \pm 30°$, $-105 \pm 55°$, $-120 \pm 40°$, and $-120 \pm 30°$, respectively. The ϕ value of $-105 \pm 55°$ was used for Pro and also for Gly, since the two alpha protons of Gly were not stereospecifically assigned. Other exceptions for AgMT were for Asn16, Asn17, Lys22, Lys35, and Cys36, where the maximum range was also used since the experimental $^3J_{HN\alpha}$ values could not be accurately defined. Exceptions for CuMT included Asn17 and Ser25 where the maximum range for ϕ was again used. Stereospecific assignments of the Cys prochiral H^{β}s permitted the determination of the χ_1 values used for both AgMT and CuMT: $180 \pm 30°$ for C7, C30, C36, C38; $-60 \pm 30°$ for C9, C11, C14, C26; $60 \pm 30°$ for C20, C24.

2.2. Structure calculations

At the outset, a decision was made to truncate the protein after the first 40 residues for the structure calculations because of the conformational dynamics present in the C-terminus that was manifested by the doubling of most of the resonances from the last 13 residues [7]. These earlier studies also showed that for both AgMT and CuMT, residues beyond N40 were disordered and not participating in any structure forming metal-thiol coordination. Therefore, the 13 C-terminal residues were excluded from the structural calculations.

Three-dimensional structures were calculated using X-PLOR3.1 [16] on a Silicon Graphics Personal Iris 4D25, and viewed using the program Insight II from Biosym Technologies. A modified Cys residue was added to the X-PLOR3.1 library and used to introduce the seven metal atoms with fixed bond length Ag-S = 2.50 Å, Cu-S = 2.25 Å [17,18,19] and fixed bond angle of 109.5° for C^{β}-S^{γ}-metal. The remaining metal-sulphur connectivities for digonal or trigonal coordination were formed using pseudo-NOEs according to the established coordination [7]. Van der Waals interactions were suitably turned off in the X-PLOR3.1 protocol to enable metals and sulphurs connected via pseudo-NOEs to approach each other within the specified separations. Variations in trigonal and digonal cluster angles were accommodated via pseudo-NOE distance constraints for metal-metal and sulphur distances for the appropriate geometry, allowing for variance in metal-S bond distance of ±0.2 Å combined with variance in S-metal-S and metal-S-metal bond angle of ±5°. For the digonally coordinated metals I and II, S-S pseudo-NOE distances of 5.00 Å and 4.50 Å were used for AgMT and CuMT, respectively. For the calculations, metal VI was assumed to have trigonal coordination with the identity of the third ligand unspecified. For trigonally coordinated metals, the pseudo-NOE distance constraints were 4.33 ± 0.45 Å for S-S and 3.22 ± 0.42 Å for Ag-Ag in AgMT, and for CuMT the corresponding constraints were 3.90 ± 0.50 Å for S-S and 2.90 ± 0.40 Å for Cu-Cu. In addition, for non-adjacent metals, metal-metal distance minima were inserted as pseudo-NOEs with a minimum of ionic radii contact. Thus, 11 metal-sulphur, 15 S-S and 21 metal-metal for a total of 47 additional pseudo-NOE distance constraints were added to the experimental NOE constraints. To insure that the geometry at the metal was approximately planar for trigonally coordinated metal ions as found in model Ag(I) and Cu(I) thiol complexes [17–19], dihedral angle constraints were used to constrain the out-of-plane angle of the metal relative to the plane of its three coordinating sulphurs to <10°. This was intentionally set to be somewhat tighter than crystallographic data for model compounds which reported excursions of up to 17° for the metal out of the plane formed by the sulphurs [18].

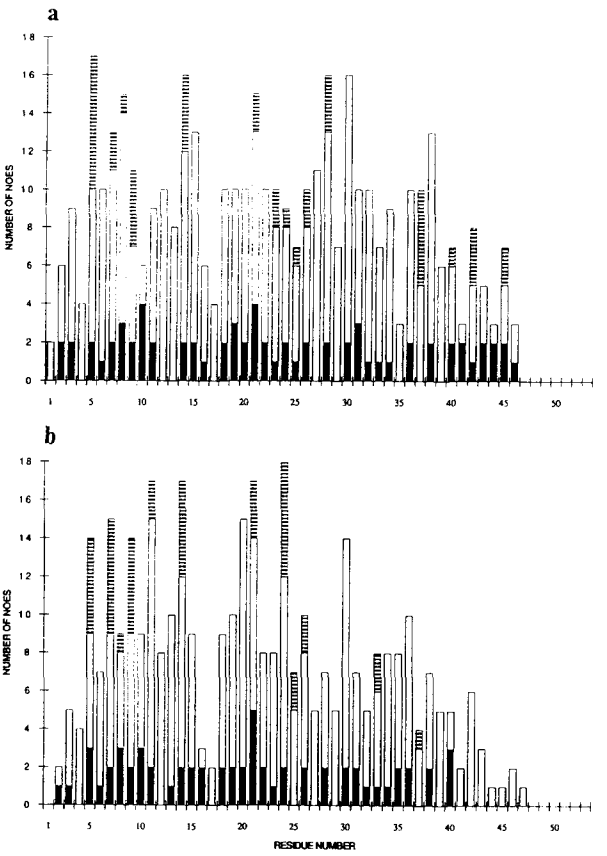

Fig. 1. Distribution of the NOE restraints used in the structural calculations for AgMT (a) and for CuMT (b). Filled bars, intraresidue NOEs; open bars, short range NOEs; striped bars, long range NOEs.

The hybrid distance geometry-dynamical simulated annealing method [20] was employed using initial structures generated from randomized ϕ and ψ torsion angles. The calculations proceeded using the substructure distance geometry protocol of X-PLOR3.1 with partial metrization [21] and only quadratic harmonic terms in the target function for minimization. Default X-PLOR3.1 parameters and weightings [16] were used in the multistage regularization [20] and molecular dynamics stages except as noted. Parameters for the final refinement were an initial annealing temperature of 500°K and a cooling stage duration of 2000 steps. For both annealing and refinement, a slow cooling timestep of 0.003 ps was used to prevent an undesirably high temperature rise during the molecular dynamics stage. The pseudo-NOEs establishing metal-Cys connectivities were given a force constant of 500 kcal · mol^{-1} · A^{-2} compared to the default force constant of 1000 kcal · mol^{-1} · A^{-2} for defined bonds between backbone atoms. For S-S and metal-metal pseudo-NOE constraints, a force constant of 1000 kcal · mol^{-1} · A^{-2} was necessary to maintain coordination angles comparable to those seen in model compounds. A force constant of 100 kcal · mol^{-1} · A^{-2} was used for all experimentally derived NOEs in both the simulated annealing and subsequent refinement calculations.

Differences in the respective calculations for AgMT and CuMT naturally included the identity and properties of the metal added to the modified Cys residue (mass, ionic radius, and metal-S bond length) and the respective experimental NOE, pseudo-NOE and dihedral angle constraints. Identical metal-Cys connectivities were assumed for CuMT as had been experimentally determined for AgMT.

Selection of final structures was based on minimum total energy and minimal NOE, dihedral and improper angle violations. A total of

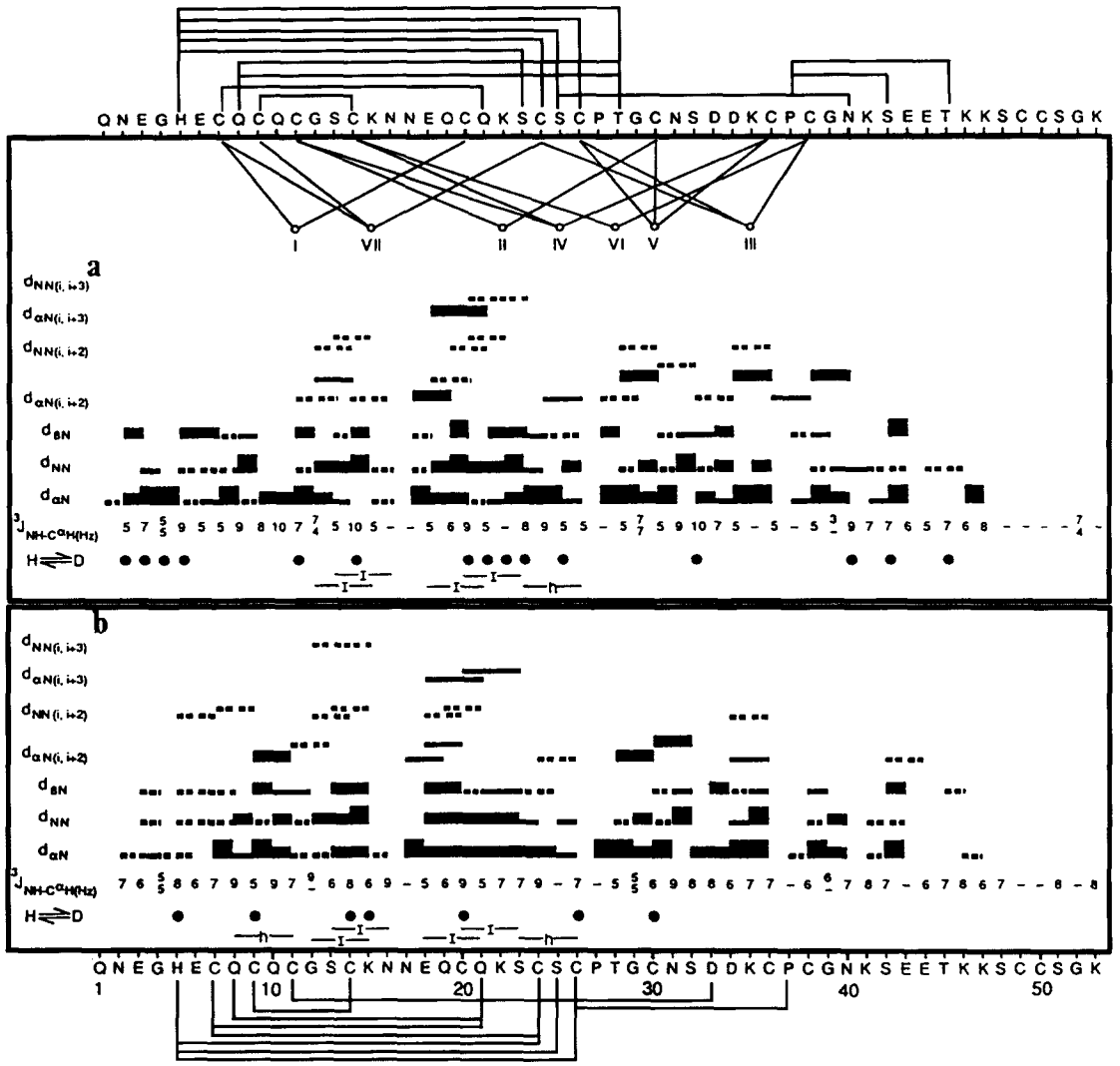

Fig. 2. Amino acid sequence and summary of the sequential and medium range NOE connectivities, $^3J_{NH\text{-}C\alpha H}$ coupling constants, and slowly exchanging amide protons (filled circles) for AgMT (a) and CuMT (b). Results from two experiments with different mixing times are shown for each MT. From the first experiment the widths of the solid lines indicate the relative strength of the NOE: weak, medium and strong. Results from the experiment with longer mixing time indicate only very weak NOEs and are shown by dashed lines. Type I and half turns are indicated, as are all of the long range NOEs and specific metal-Cys coordinate bonds determined on AgMT.

5 templates with six structures per template were calculated for both AgMT and CuMT, for a total of 30 AgMT and CuMT calculated structures. For AgMT 17/30 or 57% of the calculated structures had reasonable energies and minimal constraint violations as delineated below, while the comparable figure for CuMT was 80%, both within the success range reported for comparable X-PLOR3.0 applications [21].

3. Results

Selection criteria for final structures were minimal violations that deviated by no more than the following thresholds from the respective constraint values: 0.5 Å NOE, 0.05 Å bond length, 5° for dihedral, valence, improper and Ramachandran angles, and 10° for the out-of-plane pyramidal angle for trigonally coordinated metal ions. In addition, metal-S bonds were required to lie within ±0.2 Å of the reported X-ray metal-S bond lengths, and S-metal-S and metal-S-metal angles were required to lie within 12° of the X-ray range for model compounds [17–19]. In the final AgMT structures, the only violations of the above criteria were a small backbone valence angle violation of ≤7.5° for T28 (C^α-C-N), a sidechain valence angle violation of ≤6.6° for the P37 (C^β-C^α-C) angle and, in three of the final structures, a small, ≤5.8°, side-chain valence angle violation for C24 (C^α-C^β-S^γ). For the final structures, the angles at the metal and at the bridging sulphur are compared with model compounds in Table 1.

In Fig. 3a are shown overlays of the backbone atoms of the ten best structures of AgMT, rms fitted to the average structure for residues 5 through 38. The average rmsd for residues 5 through 38 from the average structure for backbone atoms is 0.92 ± 0.46 Å. The structures in Fig. 3a suggest the possibility of two conformers for that section of the polypeptide chain between residues 32 to 40. This structural feature in the C-terminus of AgMT would make the dominant contribution to the aforementioned rmsd. The inset of Fig. 3a depicts the relationship of His5 to the nearby crossing polypeptide strand,

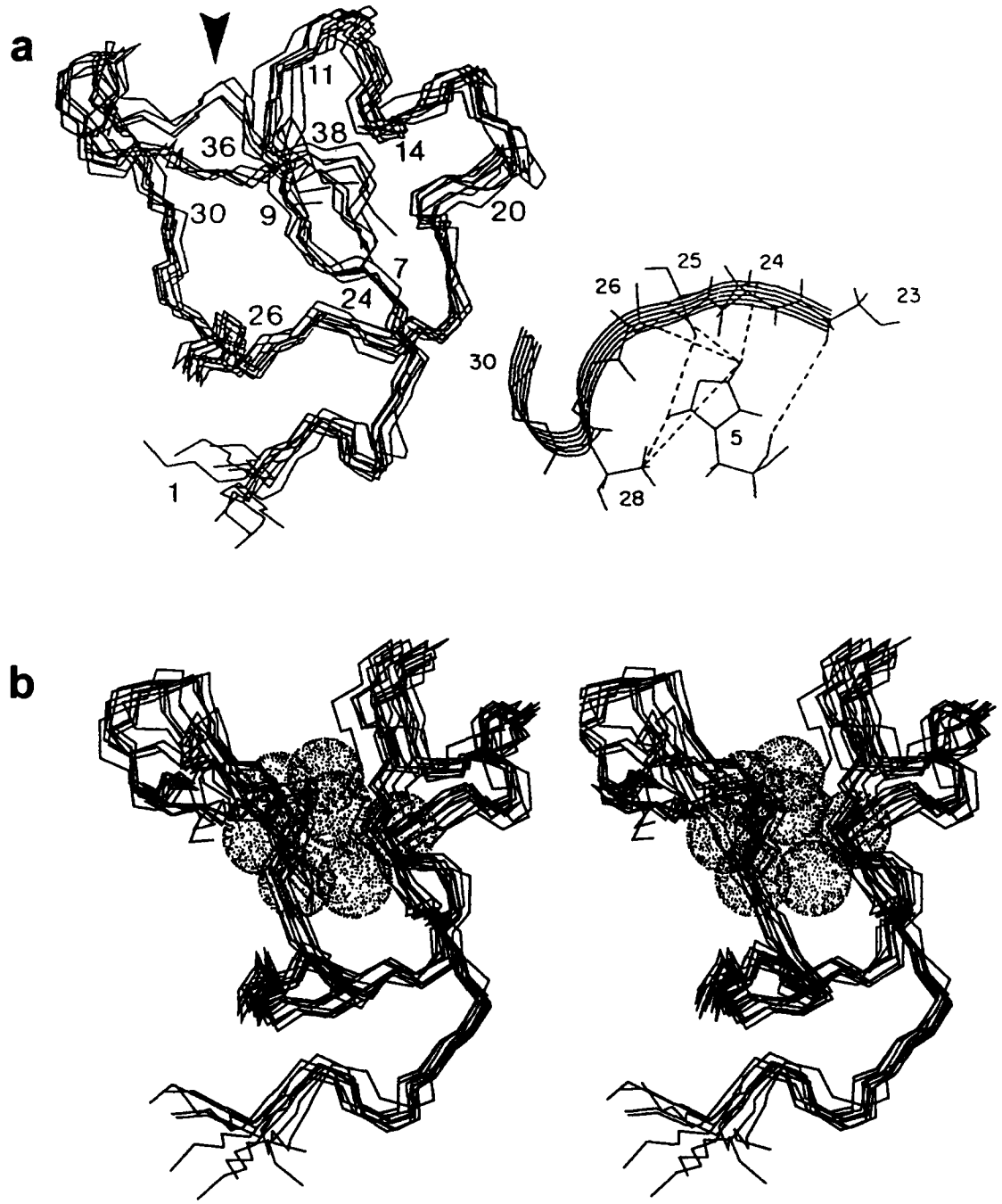

Fig. 3. Superposition of the 10 best solution structures of yeast AgMT. (a) Backbone only, rms fitted to average structure for residues 5 to 38; Cys residues are identified by number as is residue 1 at the N-terminus. The arrow highlights the region where two conformers are indicated. The inset shows a detail from the average AgMT structure with the isolated His5 residue, the segment S23-C30 represented by a backbone ribbon with full structures indicated for residues S23-C26 and T28, and the 7 long range NOEs originating at His5. b) Stereo view of structures in 3a, rotated 80° about the y axis showing the parallelism of the two large loops and the cup-like cleft between them which contains the metal cluster. Metals are shown as shaded spheres for one structure.

along with the respective long range NOEs originating at His5. Fig. 3b shows a stereo view of the same structures as Fig. 3a rotated by 80° about the vertical axis to illustrate the parallelism of the two large protein loops separated by a cup-like cleft where the metal cluster resides. With the exception of the Cys sidechains, all other sidechains lie entirely outside this cleft region. The two major loops in the protein fold are evident from the long range NOEs shown schematically in Fig. 2: H5 to the C24-C26 region, and S25 to the N40 region.

Fig. 4 plots the distribution through the amino acid sequence of the averaged rmsd per residue in the final AgMT structures from the mean structure, for backbone atoms (a) and for all non-hydrogen atoms (b). For the backbone atoms, the deviations are ≤ 1.0 Å except for residues 32–40 and residues 1 and

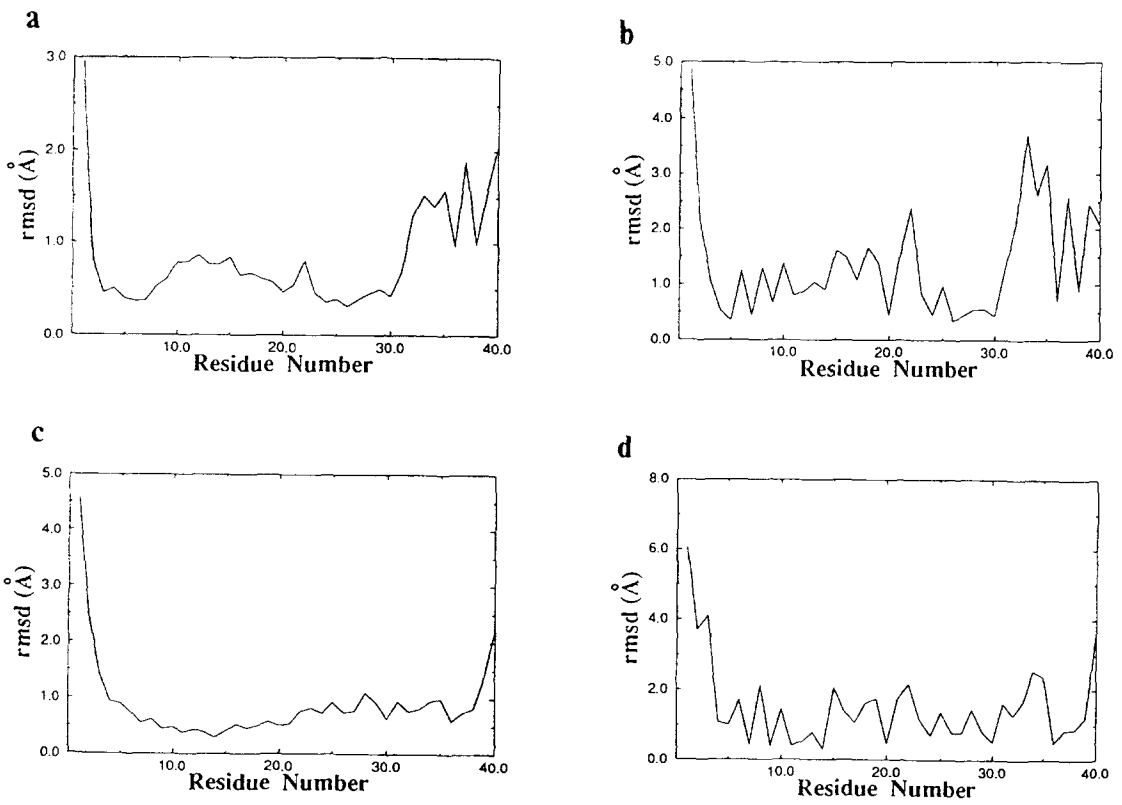

Fig. 4. Distribution through the amino acid sequence of the averaged rms deviation per residue for the final MT structures from the respective mean structures. (a) AgMT backbone atoms only; (b) AgMT all non-hydrogen atoms; (c) CuMT backbone atoms only; (d) CuMT all non-hydrogen atoms.

2 at the N-terminus. The two possible conformers beyond residue 32 seen in Fig. 3a make a large contribution to the larger rmsd seen in this region of the protein in Fig. 4a and 4b. In particular, the relatively large rmsd seen for AgMT around residue D34 coincides with the anomalously large chemical shift change of residue K35 accompanying the change of Cu(I) to Ag(I) in yeast MTs [7].

Turning to the structure of CuMT, the only violations in the final structures were a persistent sidechain χ_1 dihedral angle (N-C^{α}-C^{β}-S^{γ}) violation for Cys24 of $\leq 6.4°$ and in half of the structures, an out-of-plane or pyramidal angle violation for metal IV of $\leq 11.0°$. In the final structures, the angles at the metal and at the bridging sulphur are compared with model compounds in Table 1. The distortion seen in the calculated metal-thiol cluster dihedral and valence angles compared with model compounds is not surprising, considering substantial distortions in other reported Cys-S cluster structures [22]. Fig. 5 plots the superposition of the backbone atoms of the ten best solution structures of yeast CuMT, rms fitted to the average structure for residues 5 through 38. The inset of Fig. 5 depicts the relationship of His5 to the nearby crossing polypeptide strand, along with the respective long range NOEs originating at His5.

Table 1
Metal cluster angles (deg)

	Model compounds[a]		Calculated structures	
Trigonally coordinated:	S-metal-S	metal-S-metal	S-metal-S	metal-S-metal
Ag	104–138	70–90	96–150	64–97
Cu	105–137	70–88	93–156	61–95
Digonally coordinated:				
Ag	175		163–177	
Cu	175		146–173	

[a][17–19]

Fig. 4c plots the averaged rmsd per residue in the final CuMT structures from the mean structure for backbone atoms only, and for all non-hydrogen atoms, Fig. 4d. The rmsds are comparable with those for AgMT (Fig. 4a and b); for the backbone atoms the deviations are ≤ 1.0 Å except for residues 28, 35 and the terminal residues. The average of the rmsds for residues 5 through 38 from the average CuMT structure for backbone atoms is 0.68 ± 0.20 Å. No large increase in rmsd was observed for residues 32–40 in CuMT in contrast to AgMT which showed two conformations in this region.

The smaller Cu ionic radius of 0.91 Å and shorter metal-S bond distance predicates a more compact metal cluster and possibly a reduced protein volume for CuMT compared to AgMT. The general overall morphology with two large protein loops separated by an open cleft is, however, very similar for both. This similarity is not surprising on re-examination of Fig. 2, which exhibits only minor differences in the respective NOEs between the two proteins. An interesting difference occurs in the N-terminus where for the CuMT structures, the N-terminus residues are not constrained to lie parallel to the short strand of residues, S23-C26, as they were in AgMT, but instead show motional disorder typical of most unconstrained protein termini. This difference is explained upon closer examination of the structures which reveals that in AgMT, the histidine side

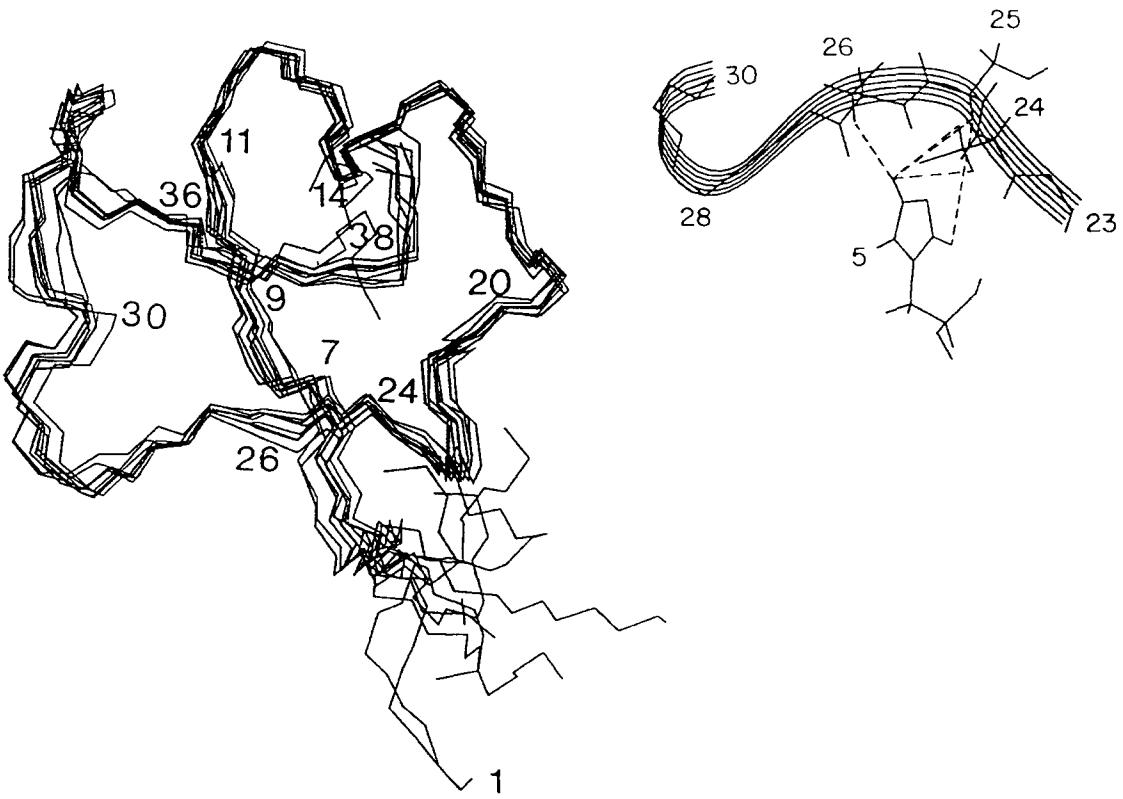

Fig. 5. Superposition of the 10 best solution structures of yeast CuMT, backbone only rms fitted to average structure for residues 5 to 38. The inset shows a detail from the average CuMT structure, with the isolated His5 residue, the strand S23-C30 indicated by a backbone ribbon with complete structures for residues C24-C26, and the 5 long range NOEs originating at His5.

chain is within hydrogen bonding distance of acceptor sites in the adjacent S23-C26 strand.

Since it appeared that the different morphologies of AgMT and CuMT at the N-terminus were related to differences in the respective number of long range NOEs from His5, a series of structures were calculated for AgMT deleting first individual and then multiples of the 7 long range NOEs connecting His5 to the crossing strand. Only when the entire set of 7 long range NOEs between His5 and the crossing strand were deleted did the resulting AgMT structures show conformational disorder at the N-terminus as observed in CuMT, indicating that the alignment in this portion of the protein appears to be the result of cooperative interactions between His5 and the strand S23-C26.

One of the unresolved questions from earlier work concerned the anomalous chemical shift for metal ion VI which appeared experimentally to be only digonally coordinated but occurred in the chemical shift range of trigonally coordinated metal ions [6,7] suggesting the existence of a third ligand. Two candidates for this missing ligand to metal VI are sulphur ligands from Cys9 and/or Cys20, however, the final calculated structures did not reveal a preference for either of these Cys ligands in terms of an acceptable metal VI-sulphur bond distance. Additional calculations were, therefore, performed deliberately connecting metal VI first to Cys9 and then alternatively to Cys20, via a metal-sulphur pseudo-NOE with appropriate adjustments in the S-S and Ag-Ag pseudo-NOEs to reflect the specific trigonal coordination of the metal VI site where before the third ligand had been unspecified. The results were that this extra coordination of either Cys9 or 20 to metal VI could be accommodated with only a few minor violations, and comparable numbers of acceptable structures were produced for both AgMT (50%) and CuMT (70%) compared to structures generated without this specified additional coordination of metal VI. These latter structures did, however, correspond very closely to the previous average structures which included, in the case of AgMT, the conformational disorder observed beyond residue 32.

The fact that this extra coordination of metal VI permitted either sulphur ligand from Cys9 or Cys20 to be coordinated with only minor violations is perhaps not too surprising in view of the ability of these proteins to accommodate a wide variety

Table 2
Potential hydrogen bonds identified from the calculated structures of yeast MT

Donor	Acceptor	AgMT distance (Å)[a]	CuMT distance (Å)[a]
H5:HN	E3:O	2.26 ± 0.16[b]	(4.71 ± 0.32)[b]
H5:Nε2	C24:O	2.47 ± 0.06	2.68 ± 0.36[c]
H5:Nε2	C24:S^{γ}	3.40 ± 0.19	(4.17 ± 0.29)
H5:Nε2	C26:O	2.80 ± 0.11	(3.22 ± 0.44)
C9:HN	C7:O	(3.08 ± 0.20)	2.39 ± 0.02[b]

[a]Hydrogen bond distances and variances are based on the 10 best structures; the numbers in parentheses indicate distances outside the acceptable range for the respective hydrogen bonds.
[b]Seen as a slowly exchanging amide proton in Fig. 2.
[c]Distances lie within the acceptable distance range for only 6 of the 10 acceptable CuMT structures.

of metal ions with different ionic radii, valence charge, metal-thiol bond distances, and metal-thiolate coordination number (e.g. Zn, Cd, Cu, Hg). The final structures for both AgMT and CuMT did, however, substantiate the much too distant location of His5 from any of the metals in the cluster for its involvement in metal coordination, in agreement with the experimental HMQC results [7].

Each of the 10 final structures for AgMT and CuMT were inspected for possible hydrogen bonds using Insight II with cut-off distances of 3.0 Å for N-H···O and 3.5 Å for N-H···S. Potential hydrogen bonds so identified which either corresponded to slowly exchanging amide protons in Fig. 2 or were associated with the His5 sidechain are tabulated in Table 2. The differences between the two MT structures are apparent: AgMT has 3 potential long range hydrogen bonds from His5 whereas the corresponding distances in CuMT exceed acceptable hydrogen bonding distances with the sole exception of H5:Nε2 to C24:O in 60% of the acceptable CuMT structures. The much larger variances in the potential hydrogen bond distances for CuMT in Table 2 reflect the disorder in its N-terminus compared with AgMT.

A summary of the structural statistics and atomic rms differences for the final AgMT and CuMT structures is given in Table 3. Atomic coordinates have been deposited with the Brookhaven Protein Data Bank for the minimized average structure of AgMT, the ensemble of 10 SA structures of AgMT, the minimized average structure of CuMT, and the ensemble of 10 SA structures of CuMT, along with the respective NMR constraints used for the structure calculations.

4. Discussion

The metal cluster of yeast MT lies in a cleft interior to the protein backbone shell with ready access of solvent only to the open side of this cleft. This may be a significant structural feature in view of the presumed functional importance of MT in metal metabolism and the reported lability of the metal ions in mammalian MT [23]. What tertiary structure exists can be attributed to the backbone twisting to accommodate the metal coordination with the deployment of the Cys in a fashion similar to the metal coordination in mammalian MT using Cys-X-Cys and Cys-XX-Cys structural motifs [24]. However, for yeast MT in contrast to the mammalian MTs, only half of the paired cysteine motifs (C-X-C) coordinate the same metal [6].

Due to the smaller ionic radius of the copper ion and its shorter metal-thiol bond, the metal cluster dimensions in CuMT are contracted slightly from AgMT and segments of the protein backbone are drawn in bowing the more rectangular outline observed for AgMT (Fig. 3a) to more of a dog-bone shape for CuMT (Fig. 5). In CuMT, the side chain of His5 is no longer in close hydrogen bonding distance to an adjacent strand reducing available constraints for the N-terminus. Experimental evidence for the importance of hydrogen bonds in stabilizing the N-terminus in AgMT is provided in Fig. 2a where four slowly exchanging amide protons are observed from residues 2 through 5 and again for residues 20 through 23 and S25. Table 2 identifies 3 potential hydrogen bonds directly linking these two regions. In contrast, in CuMT slowly exchanging backbone amide protons are found only for residues

Table 3
Structural statistics and atomic rms differences[a]

A. Structural statistics:	AgMT		CuMT	
	<SA>	$\overline{(SA)}$r	<SA>	$\overline{(SA)}$r
rms deviation from exptl distance restraints (Å) (267 for AgMT) (250 for CuMT)	0.062 ± 0.003	0.060	0.047 ± 0.005	0.044
rms deviations from exptl dihedral restraints (deg) (61)	0.718 ± 0.108	0.698	0.882 ± 0.021	1.188
rms deviations from idealized covalent geometry used within X-PLOR				
Bonds (Å) (523)	0.007 ± 0.001	0.007	0.005 ± 0.001	0.005
Angles (deg) (951)	0.982 ± 0.038	0.944	0.759 ± 0.017	0.751
Impropers (deg) (317)	0.821 ± 0.035	0.780	0.571 ± 0.012	0.597
Selected X-PLOR energies (kcal/mol)[b]				
E_{bond}	30.34 ± 1.97	27.29	16.52 ± 2.89	14.02
E_{angle}	139.83 ± 10.97	128.84	83.25 ± 3.72	81.51
$E_{improper}$	27.34 ± 2.34	24.62	13.21 ± 0.54	14.46
E_{NOE}	103.73 ± 9.50	97.52	57.05 ± 11.89	48.53
E_{cdih}	3.50 ± 0.87	3.62	3.12 ± 1.38	5.34
E_{vdw}	36.60 ± 4.65	34.91	23.17 ± 4.10	19.55

B. Atomic rms differences (Å)	<SA> vs. $\overline{SA}$ AgMT	<SA> vs. $\overline{SA}$ CuMT
All non-hydrogen atoms	1.77 ± 0.52	2.11 ± 0.50
Backbone heavy atoms	0.92 ± 0.46	0.68 ± 0.20
Metal cluster atoms (7 Ag^+ or 7 Cu^+ and 10 S)	0.51 ± 0.14	0.33 ± 0.12

[a]Notation of the NMR structure is: <SA> are the final 10 simulated annealing structures; $\overline{SA}$ is the mean structure obtained by averaging the coordinates of the individual SA structures best fit to each other: $\overline{(SA)}$r is the restrained minimized mean structure obtained by restrained regularization of the mean structure $\overline{SA}$ [20]. The number of terms for the various restraints is given in parenthesis.
[b]Energies were calculated by X-PLOR3.1 using a square well potential for the experimental NOE term (100 kcal/molA^2) and a square well quadratic energy function for the torsional potential (200 kcal/mol/rad^2).

His5 and Cys20 in the strands Q1-H5 and C20-C26. While all the protein dimensions are not affected isotropically when the larger Ag(I) ion is substitituted for Cu(I), the differences are modest and almost constant protein volume is preserved. For the ten final structures, the averaged volume is 3179 ± 90 Å^3 for AgMT and 3400 ± 63 Å^3 for CuMT as calculated with X-PLOR3.1. The slightly larger volume for CuMT despite the smaller Cu ionic radius and shorter metal-thiol bond distance compared with Ag most probably reflects the structural differences observed in the N-terminus of these two proteins as discussed above.

The short range NOE patterns along with the associated evidence of amide proton exchange rates and relative $d_{\alpha N}$ NOE strengths amongst four contiguous residues were used previously to predict four specific Type Iβ turns [7]. Upon examination of the calculated AgMT structures, the first two predicted Type Iβ turns, C11 to C14 and E18 to Q21, contain ψ_2 and ϕ_3 values within the ranges for this type of turn, −30° and −90°, respectively [5]. However, in both regions further along, P27 to C30 and D33 to C36, these angles were 30° and −140°, respectively, more characteristic of wide zeta loops [25] instead of tight Type Iβ turns.

Examining the data in Fig. 2 and the final calculated structures more closely reveals two pairs of overlapping Type I turns for both AgMT and CuMT identified for regions E18-S23 and C11-K15, supported by the $^3J_{H\alpha N}$ and d_{NN} values and the final $\psi_2\phi_3$ angles [5]. The remaining NOE motifs in Fig. 2 are indicative of a series of isolated half turns, supported by the d_{NN}, $d_{\alpha N}$ and $^3J_{H\alpha N}$ patterns and final $\psi_2\phi_3$ angles (120°, −90°) [5], at the following locations: Q8-C11 for CuMT as discussed below, and S23-C26 for both CuMT and AgMT. For the latter Cys-X-Cys motif, both Cys24 and Cys26 coordinate metal III, similar to the mammalian Cys-X-Cys motif where the backbone turns to accommodate binding of the same metal by adjacent thiols. Further evidence of the presence of these standard turns is their association with the respective slowly exchanging amide protons identified in Fig. 2, and with the potential hydrogen bonds discussed below. A third half turn structural motif is the N31-D34 segment where only one of the two AgMT conformers exhibits the standard half turn angles supported by the d_{NN} and coupling constant values.

To see whether potential acceptors could be identified for slowly exchanging protons seen in Fig. 2 additional to the two hydrogen bonds identified in Table 2, the final structures were carefully re-examined using a cutoff distance of 3.5 Å for proton-oxygen and 4.5 Å for proton-sulphur hydrogen bond distances. The results for AgMT were that acceptors for 9 of the 13 slowly exchanging amide protons in the first 40 residues could be identified. The respective potential donor-acceptor pairs identified were: 3:HN-1:O, 4:HN-2:O, 5:HN-3:O, 11:HN-9:O, 20:HN-17:O, 21:HN-18:O and/or 20:S$^\gamma$, 22:HN-20:O, 32:HN-30:S$^\gamma$, and 40:HN-38:S$^\gamma$. For CuMT, four amide proton potential acceptors were identified out of a total of 7 slowly exchanging amide protons: 9:HN-7:O and/or 7:S$^\gamma$, 20:HN-18:O, 26:HN-24:O and/or 24:S$^\gamma$, and 30:HN-27:O. These hydrogen bonding patterns are reminiscent of the Cys-X-Cys turn-related bonds in mammalian MT [24] for the Cys7-X-Cys9 and Cys24-X-Cys26 pairs in CuMT, and Cys9-X-Cys11 in AgMT. A typical shared structural feature was the identification of cysteines as the most common hydrogen bond acceptor in these proteins [24]. For the slowly exchanging amide protons whose acceptors could not be identified above, it is tempting to suggest that the acceptors might lie in the other half of a presumed dimer morphology as discussed below.

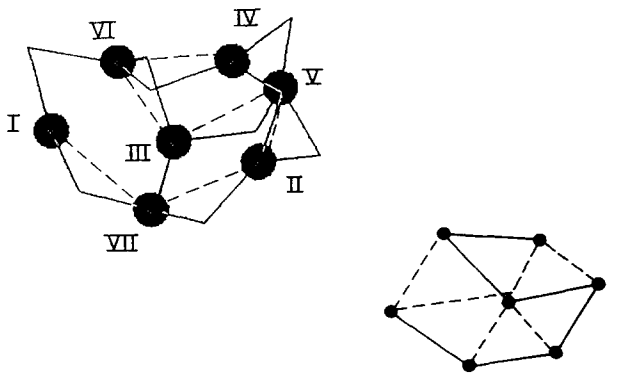

Fig. 6. Cu-S cluster in CuMT with additional coordinations of Cys9-II and Cys20-VI. The Cu ions are shown as reduced spheres. The dashed lines indicate sides of the distorted cube which are 3.3 Å in length. The inset highlights the distorted cube with the sides of unequal length indicated by dotted lines and the seven metals by filled circles.

There may be a fundamental difference in the coordination of metal II in CuMT and AgMT. Only two ligands have been identified for metal II for AgMT where Cys9 and Cys11 bind to different metals [6] and Cys9 is a terminal sulphur. It is conceivable that Cys9 may additionally be coordinated to metal II in CuMT, in which case successive coordination to metal II by Cys9 and Cys11 would necessitate the observed half turn in the backbone in the Q8-C11 segment, as in the mammalian Cys-X-Cys motif. Neither this additional coordination for metal II nor the associated half turn were observed for AgMT (Fig. 2). The proposed Cys9-II coordination for CuMT would leave Cys20 as the only available ligand for the missing ligand of metal VI. A new structure calculation used one template each for CuMT and AgMT with these Cys9-II and Cys20-VI additional coordinations as pseudo-NOEs and suitable additional Cu-Cu and S-S pseudo-NOEs for these specific coordinations. Interestingly, the resulting metal-thiol cluster for CuMT has 6 of the possible 9 adjacent Cu-Cu distances equal to 3.31 ± 0.01 Å to form a distorted cube as illustrated in Fig. 6. In contrast, structures calculated with these two additional coordinations for AgMT resulted in a more distorted cubic metal-thiol cluster with distances along the six relevant Ag-Ag edges varying from 3.25 to 3.68 Å, not unexpectedly since the requisite Q8-C11 half turn is not found in AgMT. It is interesting to note that a cubic cluster was predicted for the Cu-S center of yeast CuMT [27] on the basis of EXAFS data even though this was based on a Cu_8S_{12} stoichiometric complex.

A still unresolved question in yeast MT is the role of cysteine residues C49 and C50, which are not involved in metal coordination in Ag substituted wildtype MT but are somehow correlated with the observed doubling of the backbone proton resonances from residue K41 onward in the C-terminus in both AgMT and CuMT [7]. A possible explanation of the MT C-terminus resonance doubling may be monomer-monomer interaction in the formation of a dimer morphology which is localized to the last 13 C-terminus residues. In this model, C49-C50 are critically positioned to facilitate dimerization; their removal in the truncated mutant, AgT48, removes the

observed resonance doubling from the last 13 residues without affecting the metal stoichiometry. A similar doubling of C-terminal resonances in the spectra of wild-type Mnt repressor of *Salmonella* bacteriophage P22 relative to a C-terminal deletion mutant Mnt (1–76) is related to the region of dimer-dimer contact in this tetrameric protein [26]. In yeast MT, therefore, it seems that the first 40 residues from the N-terminus form the core of the protein containing a cluster of 7 metals and the C-terminus serves to initiate protein-protein interactions. Of particular note is the fact that the 6-mer portion of the yeast protein sequence containing C49-C50 (KKSCCS) is found in all mammalian MTs. In mammalian MT, however, this same sequence connects the α and β domains, e.g. rat liver MT K30-S35, where residues K30-K31-S32 are the linker region and the double cysteine residues (C33 and C34) mark the beginning of the α domain. It is possible that yeast MT represented a transition in the evolution of higher MTs, where for yeast a dimer morphology served as the prototype of the later two-domain mammalian MTs.

It is noteworthy that the primary structure for CuMT is strikingly similar to that for the ACE1 metalloprotein which regulates yeast MT gene expression [11]. If the ACE1 structures parallel those observed for the related MTs, then the volume and hence relative protein compactness would be conserved between Ag and CuACE1, contrary to predictions of a less compact structure for AgACE1 [11]. Differences in the respective ACE1 structures would be confined to minor changes in N-terminus morphology and the numbers and locations of hydrogen bonds as observed in the structures of AgMT and CuMT. However, if the Cys9-Cys11 half turn distinction between the CuMT and AgMT structures is homologous to a difference in AgACE1 and CuACE1 with its implications for metal cluster symmetry and coordination, then this could possibly explain the observed differences in spectroscopy, stability, metal binding cooperativity and DNA affinity between the ACE1 Cu and Ag proteins.

Acknowledgement: The authors thank Prof. D.R. Winge of the Department of Biochemistry and Medicine, University of Utah Medical Center, Salt Lake City, Utah, for providing the protein for the NMR studies which made the present structure calculations possible. They also thank Prof. Axel Brünger for helpful discussions on the use of X-PLOR and Kevin Gardner for sharing software that facilitated structure analysis. Very thoughtful criticisms and comments from Yuxin Hua in this laboratory are also gratefully acknowledged. This work was supported in part by National Institutes of Health grant DK18778. NMR instrumentation and computational facilities were provided from NIH (RR03475), NSF (DMB8610557) and ACS (RD259).

References

[1] Kägi, J.H.R. and Kojima, Y. (1987) in: Proceedings of the 2nd International Meeting on Metallothioneins and other Low Molecular Weight Metal-Binding Proteins, Zürich, Aug 21–25, 1985 (Kägi, J.H.R. and Kojima, Y., Eds.) Vol. 52, pp. 25–61, Birkhäuser Verlag, Basel.
[2] Hamer, D.H., Theile, D.J. and Lemontt, J.E. (1985) Science 228, 685–690.
[3] Bremner, I. (1987) in: Proceedings of the 2nd International Meeting on Metallothioneins and other Low Molecular Weight Metal-Binding Proteins, Zürich, Aug 21–25, 1985 (Kägi, J.H.R. and Kojima, Y., Eds.) Vol. 52, pp. 81–107, Birkhäuser Verlag, Basel.
[4] Byrd, J., Berger, R.M., McMillin, D.R., Wright, C.F., Hamer, D. and Winge, D.R. (1988) J. Biol. Chem. 263, 6688–6694.
[5] Wüthrich, K. (1986) NMR of Proteins and Nucleic Acids, Wiley, New York.
[6] Narula, S.S., Mehra, R.K., Winge, D.E. and Armitage, I.M. (1991) J. Am. Chem. Soc. 113, 9354–9358.
[7] Narula, S.S., Winge, D.E. and Armitage, I.M. (1993) Biochemistry 32, 6773–6787.
[8] Dameron, C.T., George, G.N., Arnold, P., Santhanagopalan, V. and Winge, D,R. (1993) Biochemistry 32, 7294–7301.
[9] Casas-Finet, J.R., Hu, S., Hamer, D. and Karpel, R.L. (1992) Biochemistry 31, 6617–6626.
[10] Fürst, P. and Hamer, D. (1989) Proc. Natl. Acad. Sci., USA 68, 5267–5271.
[11] Fürst, P., Hu, S., Hackett, R. and Hamer, D. (1988) Cell 55, 705–717.
[12] Williamson, M.P., Havel, T.F. and Wüthrich, K. (1985) J. Mol. Biol. 182, 295–315.
[13] Clore, G.M., Nilges, M., Sukumaran, D.K., Brünger, A.T., Karplus, M. and Gronenborn, A.M. (1986) EMBO J. 5, 2729–2735.
[14] Clore, G.M., Gronenborn, A.M., Nilges, M. and Rycan, C.A. (1987) Biochemistry 26, 8012–8013.
[15] Wagner, G., Braun, W., Havel, T.F., Schaumann, T., Go, N. and Wüthrich, K. (1987) J. Mol. Biol. 196, 611–639.
[16] Brünger, A.T. (1993) X-PLOR Version 3.1 Manual, Yale University Press, New Haven, CT, USA.
[17] Dance, I.G. (1976) J. Chem. Soc., Chem. Commun. 103–4.
[18] Dance, I.G. (1978) Aust. J. Chem. 31, 2195–206.
[19] Dance, I.G. (1981) Inorg. Chem. 20, 1487–92.
[20] Nilges, M., Clore, G.M. and Gronenborn, A.M. (1988) FEBS Lett. 229, 317–324.
[21] Kuszewski, J., Nilges, M. and Brünger, A.T. (1992) J. Biomol. NMR 2, 33–56.
[22] Winge, D.R., Dameron, C.T., George, G.N., Pickering, I.J. and Dance, I.G. (1993) in: Bioinorganic Chemistry of Copper, Edited by K.H. Karlin and Z. Tyeklár, Chapman and Hall, NY.
[23] Nettesheim, D.G., Engeseth, H.R. and Otvos, J.D. (1985) Biochemistry 24, 6744–6751.
[24] Robbins, A.H., McRee, D.E., Williamson, M., Collett, S.A., Xuong, N.H., Furey, W.F., Wang, B.C. and Stout, C.D. (1991) J. Mol. Biol. 221, 1269–1293.
[25] Ring, C.S., Kneller, D.G., Langridge, R. and Cohen,F.E. (1992) J. Mol. Biol. 224, 685–699.
[26] Burgering, M.J.M., Boelens, R., Gilbert, D.E., Breg, J.N., Knight, K.L., Sauer, R.T. and Kaptein, R. (1994) Biochemistry 33, 15036–15045.
[27] George, G.N., Byrd, J. and Winge, D.R. (1988) J. Biol. Chem. 263, 8199–8203.